Journal of Power Sources 253 (2014) 332–341

Contents lists available at ScienceDirect

Journal of Power Sources

journal homepage: www.elsevier.com/locate/jpowsour

Corrosion behaviour of austenitic stainless steel as a function of methanol concentration for direct methanol fuel cell bipolar plate

Lixia Wang, Bin Kang, Na Gao, Xiao Du, Linan Jia, Juncai Sun*

Institute of Materials and Technology, Dalian Maritime University, Dalian 116026, China

HIGHLIGHTS

- Corrosion behaviour of AISI 304 stainless steel in DMFC anodic environment as a function of methanol concentrations.
- Electrochemical tests show that methanol decreases the corrosion rate of 304 SS.
- Passive film formed on 304 SS has a duplex electronic structure.
- The passive film is composed of an external n-type and an internal p-type semiconductor layer.
- The increase of methanol concentration decreases the surface conductivity of 304 SS.

ARTICLE INFO

Article history:
Received 23 August 2013
Received in revised form
6 December 2013
Accepted 9 December 2013
Available online 25 December 2013

Keywords:
Direct methanol fuel cell
Bipolar plate
Austenitic stainless steel
Corrosion resistance
Interfacial contact resistance

ABSTRACT

The corrosion behaviour of an AISI 304 stainless steel (304 SS) is investigated in aqueous acid methanol solutions (0.5 M H_2SO_4 + 2 ppm HF + x M CH_3OH, x = 0, 1, 5, 10 and 20) at 50 °C to simulate the varied anodic operating conditions of direct methanol fuel cells. Electrochemical measurements including potentiodynamic polarisation, potentiostatic polarisation and electrochemical impedance spectroscopy tests, are employed to analyse the corrosion behaviour. The results reveal that the corrosion resistance of 304 SS is enhanced in solutions with higher methanol content. Scanning electron microscopy and inductively coupled plasma atomic emission spectrometry data indicate that the surface corrosion on 304 SS is alleviated when the methanol concentration is increased. According to the X-ray photoelectron spectroscopy and Mott–Schottky analyses, the passive films formed on the 304 SS after potentiostatic tests in all the test solutions are composed of a duplex electronic structure with an external n-type semiconductor layer and an internal p-type semiconductor layer. Further analyses of the surface conductivity conducted by measuring the interfacial contact resistance between the 304 SS and carbon paper reveal that the passive film formed in the solution with higher methanol content exhibits lower conductivity.

1. Introduction

Polymer electrolyte membrane fuel cells, which convert chemical energy into electric power via catalytically electrochemical reactions, have gained extensive attention as new power sources due to their relatively simple operating mechanisms, high efficiency and low emissions [1–4]. For portable applications of polymer electrolyte membrane fuel cells, there are two main choices of fuels: hydrogen and methanol. Hydrogen can be stored in forms of metal hydrides or compressed gases. The metal hydrides possess large specific weights, and the compressed gases occupy relatively large volumes. Moreover, the compressed gaseous hydrogen has potential safety issues when used in most portable electronics. Compared to hydrogen, liquid methanol has greater volumetric and gravimetric energy density, making it much easier to store, transport and replenish. These advantages make direct methanol fuel cells (DMFCs) suitable for meeting the rapidly growing need for portable power sources in devices, such as mobile phones, notebooks, and portable electronic devices [5–8].

Bipolar plates are one of the most crucial components in the DMFC stack, constituting 80–85% of the total weight and 25–45% of the total cost of the fuel cell stack [9–11]. A bipolar plate physically separates the individual cells in the stack, electrically connects cell units and uniformly distributes the fuel and oxidant gas over the electrode reaction surface. Various materials have been screened as bipolar plates in recent years. Stainless steels are potential candidates for bipolar plate materials due to their good electrochemical

* Corresponding author. Fax: +86 411 84727959.
E-mail address: sunjc@dlmu.edu.cn (J. Sun).

0378-7753/$ – see front matter
http://dx.doi.org/10.1016/j.jpowsour.2013.12.043

stability, high levels of electrical and thermal conductivity as well as good machinability.

During DMFC operation, the electrochemical reactions involved are expressed as follows [12,13]:

$$\text{Anodic reaction: } CH_3OH + H_2O \rightarrow CO_2 + 6H^+ + 6e^- \quad (1)$$

$$\text{Cathodic reaction: } 3O_2 + 12H^+ + 12e^- \rightarrow 6H_2O \quad (2)$$

$$\text{Overall reaction: } 2CH_3OH + 3O_2 \rightarrow 2CO_2 + 4H_2O \quad (3)$$

Both the performance and the efficiency of the DMFC are strongly influenced by the methanol concentration due to methanol crossover. The DMFC usually shows a higher power density when fed with lower concentrations of methanol solutions (1–4 M) [7,14–17]. Nevertheless, a more concentrated methanol solution helps enhance the specific weight energy density of the DMFC system. More concentrated methanol solutions can be utilised by modifying existing membranes or employing components that prevent methanol crossover [18–20]. Furthermore, during fuel cell operation ions such as H^+, SO_4^{2-} and F^- can be released from the perfluorosulphonic acid membrane [21,22]. Therefore, according to the above description, the bipolar plates are exposed to aqueous solutions containing acid and methanol. As previously reported [23,24], the corrosion behaviour of stainless steel in organic solvents is different from that in aqueous solutions, due to differences in the electric and binding interactions between the metal and solvent as well as in the physicochemical properties such as the dielectric constant, viscosity and solubility of the reactants or products. The corrosion behaviour of stainless steel in non-aqueous methanol solutions has been extensively studied based on the effect of a small amount of water (typically less than 0.1 wt%) on corrosion, passivation and pitting processes [24–28]. However, the influence of methanol concentration on the corrosion behaviour of stainless steel-based bipolar plates in acidic aqueous solutions is not yet completely understood. Therefore, in this paper, the corrosion performance and the surface conductivity of an austenitic stainless steel AISI 304 were investigated using an aqueous acid methanol solution (0.5 M H_2SO_4 + 2 ppm HF + x M CH_3OH, x = 0, 1, 5, 10, and 20) while varying the methanol concentration to simulate the varied anodic operating conditions of DMFCs. The primary aim of this work is to offer fundamental information regarding the research and development of stainless steel bipolar plates for DMFCs.

2. Experimental section

2.1. Sample preparation

In this work, an austenitic stainless steel (AISI 304) was chosen as metal bipolar plates for DMFCs. The nominal compositions of the applied AISI 304 stainless steel (304 SS) are presented in Table 1. Stainless steel sheets with thickness of 1.5 mm were cut into 10 mm × 10 mm samples (with an area of 1 cm^2). Afterwards, the samples were ground with #360, #500, #800, #1000 and #1500 grit silicon carbide abrasive papers, polished mechanically with 0.25 μm alumina paste, rinsed with acetone in an ultrasonic cleaner, and dried at room temperature.

Table 1
Chemical composition of AISI 304 stainless steel (wt%).

Metal	C	Cr	Ni	Si	S	P	Mn	Fe
304 SS	0.049	18.20	8.66	0.58	0.007	0.021	1.05	Balance

2.2. Electrochemical measurements

Solutions of 0.5 M H_2SO_4 + 2 ppm HF + x M CH_3OH (x = 0, 1, 5, 10 and 20) at 50 °C were utilised to examine the effect of methanol concentration on the corrosion behaviour of 304 SS under DMFC anodic operating conditions. The temperature of the electrochemical tests was maintained with an isothermal bath. The electrochemical experiments were performed using a computer-controlled CHI660C electrochemical workstation. A typical three-electrode system composed of a platinum sheet (as the auxiliary electrode), the 304 SS samples (as the working electrode), and a saturated calomel electrode (SCE, as the reference electrode) was used for the electrochemical measurements. All the potentials reported are relative to SCE unless otherwise specified. Before test, each sample was embedded in a polytetrafluoroethylene (PTFE) holder that accurately exposed the fixed surface of the sample to the corrosion solutions.

To evaluate the basic corrosion behaviour of the 304 SS in solutions of 0.5 M H_2SO_4 + 2 ppm HF + x M CH_3OH (x = 0, 1, 5, 10 and 20), potentiodynamic polarisation measurements were carried out. At the beginning of potentiodynamic test, each sample was stabilised at an open circuit potential (OCP) for 30 min, then started potential sweep from −0.2 V vs OCP to 1.2 V at a scanning rate of 1 mV s^{-1}. To investigate the performance of 304 SS under DMFC anodic operation conditions, potentiostatic tests were performed. In these tests, the samples were also stabilised at OCP for 30 min, the potential of −0.1 V was then applied, and the current–time curves were recorded for 10 h. To quantify the dissolved metallic Fe, Ni, and Cr ions produced during the potentiostatic process, all the test solutions (approximately 100 ml for each test) were collected after the 10 h potentiostatic tests. Inductively coupled plasma atomic emission spectrometry (ICP–AES) (Optima 2000 DV) was used to detect the Fe, Cr, and Ni ions dissolved in the collected solutions. After the 10 h potentiostatic tests, electrochemical impedance spectroscopy (EIS) was carried out over a frequency range from 100 kHz to 10 mHz with a potential amplitude of 10 mV. The impedance spectra were interpreted with an equivalent circuit that was used to fit the experimental EIS data. The process of fitting was carried out with a ZSimpWin software.

The semi-conductive properties of passive films formed on surface of stainless steel can be determined by the flat band potential E_{fb} and doping density extracted from Mott–Schottky plots. The Mott–Schottky analysis was carried out from −0.5 V to 0.2 V at a scanning rate of 50 mV per step with a frequency and an amplitude of 500 Hz and 5 mV, respectively.

2.3. Surface morphology and passive film analysis

After the 10 h potentiostatic tests in solutions of 0.5 M H_2SO_4 + 2 ppm HF + x M CH_3OH (x = 0, 1, 5, 10 and 20), the surface morphology of the 304 SS samples was observed via scanning electron microscopy (SEM) (SUPRA 55 SAPPHIRE, ZEISS), and the composition of the passive film formed on the samples was identified qualitatively and quantitatively using X-ray photoelectron spectroscopy (XPS). The XPS analysis was carried out in an ESCALAB 250 electron spectrometer using an Al Kα source (1486.8 eV). The depth profile was achieved by Ar etching with ion energy of 0.5 keV. The sputtering rate of the Ar-ion gun was determined to be approximately 0.06 nm s^{-1} under the applied conditions.

The interfacial contact resistance (ICR) was measured using the method proposed by Wang et al. [3], which was detailed in Refs. [4,11].

3. Results and discussion

3.1. Potentiodynamic polarisation

The potentiodynamic polarisation curves of 304 SS in 0.5 M H_2SO_4 + 2 ppm HF + x M CH_3OH (x = 0, 1, 5, 10 and 20) solutions with varied methanol concentrations are shown in Fig. 1, and the corresponding corrosion results obtained from the polarisation curves are displayed in Table 2. It is observed that the 304 SS shows typical potentiodynamic polarisation curves for an austenitic stainless steel, which can be divided into five regions, namely cathodic, active, active–passive transition, passive and transpassive regions, in all the test solutions. The corrosion potentials (E_{corr}) shift towards the positive direction with increasing methanol concentrations in the test solutions. A higher corrosion potential reflects a lower corrosion tendency. Therefore, methanol is most likely important for increasing the thermodynamic stability of the 304 SS in 0.5 M H_2SO_4 + 2 ppm HF acid solutions. Moreover, the active–passive transition peak (corresponding to the critical current density I_c) and the passive current density (I_{pas}) decrease when the methanol concentration increases, indicating that the 304 SS is passivated more readily in solutions with higher methanol concentrations. This result is reasonable because the solubility of oxygen (O_2) is higher in pure methanol than that in pure water (for example, 0.227 cm^3 and 0.027 cm^3 at 1 atom 298 K [29] for methanol and water, respectively). The higher the methanol concentration, the more oxygen could be dissolved in the test solutions. The dissolved oxygen facilitates the passivation of stainless steel. At approximately 0.9 V, the current densities increase rapidly again due to the transpassivation, which is attributed to the formation of high-valence chromium [30]. The pitting potential (E_{pit}) clearly increases when the methanol concentration increases. The corrosion current densities ($I_{(-0.1\ V)}$) of 304 SS at −0.1 V, which corresponds to the typical anodic operating potential of a DMFC (marked in Fig. 1), are also summarised in Table 2. The corrosion current density at −0.1 V decreases when the methanol concentration increases, and in the solution containing 20 M methanol, $I_{(-0.1\ V)}$ reaches 3.54 μA cm^{-2}, representing one order of magnitude lower than that (22.96 μA cm^{-2}) in the solution without methanol. These results suggest that methanol can inhibit corrosion of the 304 SS in the 0.5 M H_2SO_4 + 2 ppm HF acid solutions. The effects of methanol on the rate of corrosion can be attributed to its ability to lower the mobility of the protons. Due to the preferential protonation of water in aqueous methanol solutions, the protons reside on the water molecules in the form of H_3O^+ instead of $H^+(CH_3OH)$ [31]. According to the Grothuss-type hopping mechanism, the H_3O^+ cannot hop to methanol due to the higher energy; instead, these species can hop to water molecules in the test solutions to conduct the protons [32]. When the methanol content increases in the test solutions, the water content decreases relatively, thus decreasing the proton conductivity and diffusion coefficient. Because the corrosion rate of stainless steel in aqueous acid methanol solution is limited by the rate of proton reduction, which is partially limited by mass transport [33], the methanol reduces the corrosion rate by decreasing the proton mobility.

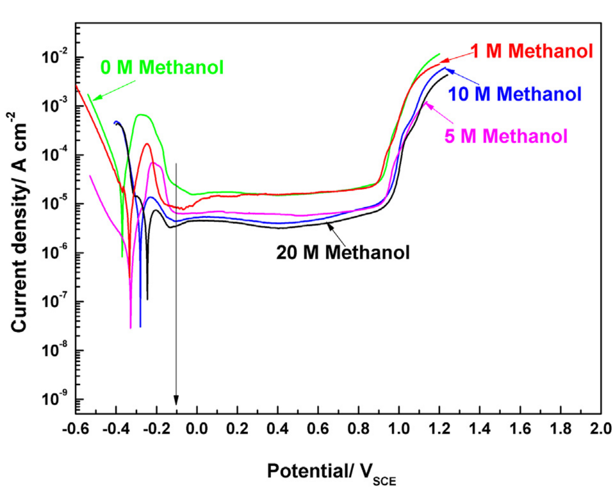

Fig. 1. Potentiodynamic polarisation plots for 304 SS in 0.5 M H_2SO_4 + 2 ppm HF + x M CH_3OH (x = 0, 1, 5, 10 and 20) solutions at 50 °C.

Table 2
Polarisation parameters of 304 SS in 0.5 M H_2SO_4 + 2 ppm HF + x M CH_3OH (x = 0, 1, 5, 10 and 20) solutions at 50 °C.

Methanol content	E_{corr} (V_{SCE})	$I_{(-0.1\ V)}$ (μA cm^{-2})	I_c (μA cm^{-2})	I_{pas} (μA cm^{-2})	E_{pit} (V_{SCE})
0 M	−0.371	22.96	666.0	15–20	0.850
1 M	−0.334	8.13	168.0	13–20	0.910
5 M	−0.303	6.38	69.5	8–12	0.912
10 M	−0.281	4.41	13.6	6–10	0.913
20 M	−0.246	3.54	7.4	5–9	0.967

3.2. Potentiostatic polarisation

To examine the stability of the 304 SS during DMFC operation, the potentiostatic tests were conducted in 0.5 M H_2SO_4 + 2 ppm HF + x M CH_3OH (x = 0, 1, 5, 10 and 20) solutions at 50 °C for 10 h. The current densities of the 304 SS as a function of time measured at −0.1 V_{SCE} are shown in Fig. 2. In all cases, the transient current densities decrease sharply at the beginning of the potentiostatic tests and afterwards to reach the steady-state current densities. The variations in the current density are primarily related to the passivation procedure because the applied potential (−0.1 V) is in the passivation region in the potentiodynamic polarisation curve, as shown in Fig. 1. The decrease in current density with extending of time reflects the nucleation and growth of the passive film that protects the stainless steel from further corrosion in acid solutions. Once the passive film covers the entire surface of the 304 SS, the growth and dissolution of the passive film reaches a dynamic equilibrium state, and the current density sustaining the passivation decreases to a relatively lower value. The stable current density for 304 SS that was measured in acid solutions without methanol is approximately 6–8 μA cm^{-2}, whereas the value in the solution containing 1 M methanol is 5–6 μA cm^{-2}. When the methanol concentration increases to 5 M, the stable current density decreases to approximately 1–3 μA cm^{-2}, indicating a lower corrosion rate. For the test solutions containing 10 M and 20 M methanol, the current density stabilises to positive and negative oscillation states from −1.5 to 1.5 μA cm^{-2} and from −2 to 1.5 μA cm^{-2}, respectively. The positive current density is related to the anodic dissolution of 304 SS and the negative current density is related to the reduction of proton during the potentiostatic test. Sakakibara et al. [34] studied the corrosion of iron in anhydrous methanol solutions and noted that the product of iron in anhydrous methanol was ferrous methoxide ($Fe(OCH_3)_2$) which was sparingly soluble in anhydrous methanol and deposited on the surface of the corroding iron. In the present corrosion system, ferrous methoxide is expected to appear on the surface of the 304 SS due to the reaction between methanol and the partial iron of the 304 SS. Because the ferrous methoxide forms a barrier that protects the passive film from dissolution, the dissolution rate of 304 SS in the test solution will decrease and the positive current density will

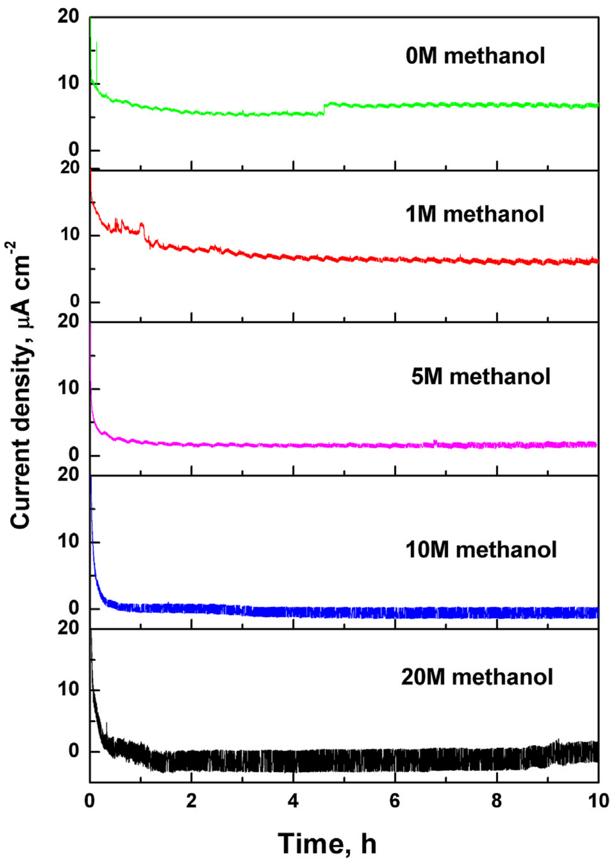

Fig. 2. Time–current density relationship for the 304 SS in 0.5 M H_2SO_4 + 2 ppm HF + *x* M CH_3OH ($x = 0$, 1, 5, 10 and 20) solutions at 50 °C.

decrease accordingly. When the anodic dissolution of 304 SS is restrained, the reduction of H^+ gradually becomes the primary electrochemical reaction. The negative current arises due to the reduction of H^+:

$$2H^+ + 2e^- \rightarrow H_2 \tag{4}$$

As aforementioned, methanol reduces the conductivity and diffusion coefficient of the protons in the test solution. When the methanol concentration in the test solution is 10 M or 20 M, the reduction rate of H^+ on the 304 SS surface is faster than its diffusion in the solution. Therefore, the hydrogen evolution gradually reduces because there is not enough H^+ on the 304 SS surface to facilitate this process, gradually reducing the absolute value of the current density to zero. Moreover, the ferrous methoxide is unstable and ferrous oxide might form due to the decomposition of ferrous methoxide [34]:

$$Fe(OCH_3)_2 \rightarrow FeO + CH_3OCH_3 \tag{5}$$

In low pH solutions, such as 0.5 M H_2SO_4, FeO may react with H_2SO_4 and dissolve; meanwhile, the anodic dissolution of 304 SS gradually becomes the primary electrochemical reaction, which results in an increase in the corrosion current density. The above process repeats continuously, causing oscillations in the current density from positive to negative. Furthermore, the current density shows more obvious oscillations from positive to negative in the solutions with higher methanol concentrations.

The surface morphologies of the 304 SS after the potentiostatic tests in 0.5 M H_2SO_4 + 2 ppm HF + *x* M CH_3OH ($x = 0$, 1, 5, 10 and 20) solutions with increasing methanol concentrations at 50 °C were observed by SEM, as depicted in Fig. 3(a)–(e). It is clearly seen that, the corrosion is significant for the 304 SS samples corroded in the acid solution containing 0 M and 1 M methanol, as presented in Fig. 3(a) and (b), respectively. The samples suffer from inhomogeneous corrosion during the potentiostatic tests, and intergranular corrosion, pitting as well as internal micro-stress corrosion are observed when the methanol concentration is 0 M or 1 M. Furthermore, the sample is corroded more severely in the acid solution without methanol. Intergranular corrosion and internal micro-stress corrosion are alleviated when the methanol concentration increases to 5 M, as shown in Fig. 3(c). Only pitting can be observed on the surface of the 304 SS placed in the test solution containing 10 M or 20 M methanol. Moreover, 304 SS suffers from more serious pitting corrosion in the acid solution containing 10 M methanol than that undergone by the sample placed in 20 M methanol. In the potentiostatic tests, the decrease in the corrosion current density of 304 SS with the increase in the methanol concentration indicates that 304 SS undergoes less corrosion when the methanol content is higher, validating the SEM results.

The metallic ions released from the corrosion of the bipolar plates may migrate towards the electrode catalysts [35], severely degrading the performance of the DMFC stack. The concentrations of the released metallic ions in the test solutions were measured by ICP–AES after 10 h potentiostatic tests in 0.5 M H_2SO_4 + 2 ppm HF + *x* M CH_3OH ($x = 0$, 1, 5, 10 and 20) solutions with varied methanol concentrations at 50 °C. Table 3 presents the Fe, Cr, Ni, and the total dissolved metallic-ion concentrations in the five different solutions. After comparing the metallic ions in each solution, the concentration of Fe ions is revealed to be the highest in each of the five different test solutions, implying that the Fe in the 304 SS is dissolved selectively [36]. When comparing the total amount of metallic ions in the five different test solutions, it is observed that the total metallic ions released from 304 SS is the highest in the test solution without methanol due to the severe inhomogeneous corrosion of 304 SS shown in the SEM images (Fig. 3(a)). It is also noted that the concentration of the total metallic ions dissolved in the test solution decreased when increasing the methanol concentration. The ICP–AES data demonstrate that methanol is critical for retarding the corrosion of 304 SS in DMFC anodic operating conditions.

3.3. Electrochemical impedance spectroscopy

Electrochemical impedance spectroscopy (EIS) is an effective technique for analysing the corrosion processes of electrical conductors in electrolytes due to the low amplitude of the perturbation signal, which allows for the monitoring of the electrode electrochemical behaviour with time without altering its surface properties. Fig. 4(a) shows the Nyquist plots for the 304 SS acquired in 0.5 M H_2SO_4 + 2 ppm HF + *x* M CH_3OH ($x = 0$, 1, 5, 10 and 20) solutions with varied methanol concentrations. Within the frequency range of the measurements (100 kHz to 10 mHz), all the Nyquist plots display one depressed semicircle in the high frequency zone and a Warburg diffusion tail in the low frequency zone. The appearance of the Warburg impedance indicates a diffusion-controlled electrochemical system, i.e. diffusion reactions have occurred on the passivated electrodes. The Bode plots of the 304 SS are shown in Fig. 4(b) and (c). In the higher frequency region ($f > 10^3$ Hz), log|*Z*| tends to stabilise, while the phase angle falls rapidly with increasing frequencies. This behaviour is a typical resistive response and corresponds to the solution resistance (R_s) [37]. A linear relationship between log *f* and log |*Z*| can be observed and the phase angle reaches its maximum value in the medium frequency range (1 Hz to 10^3 Hz). Typically, the slopes in the linear

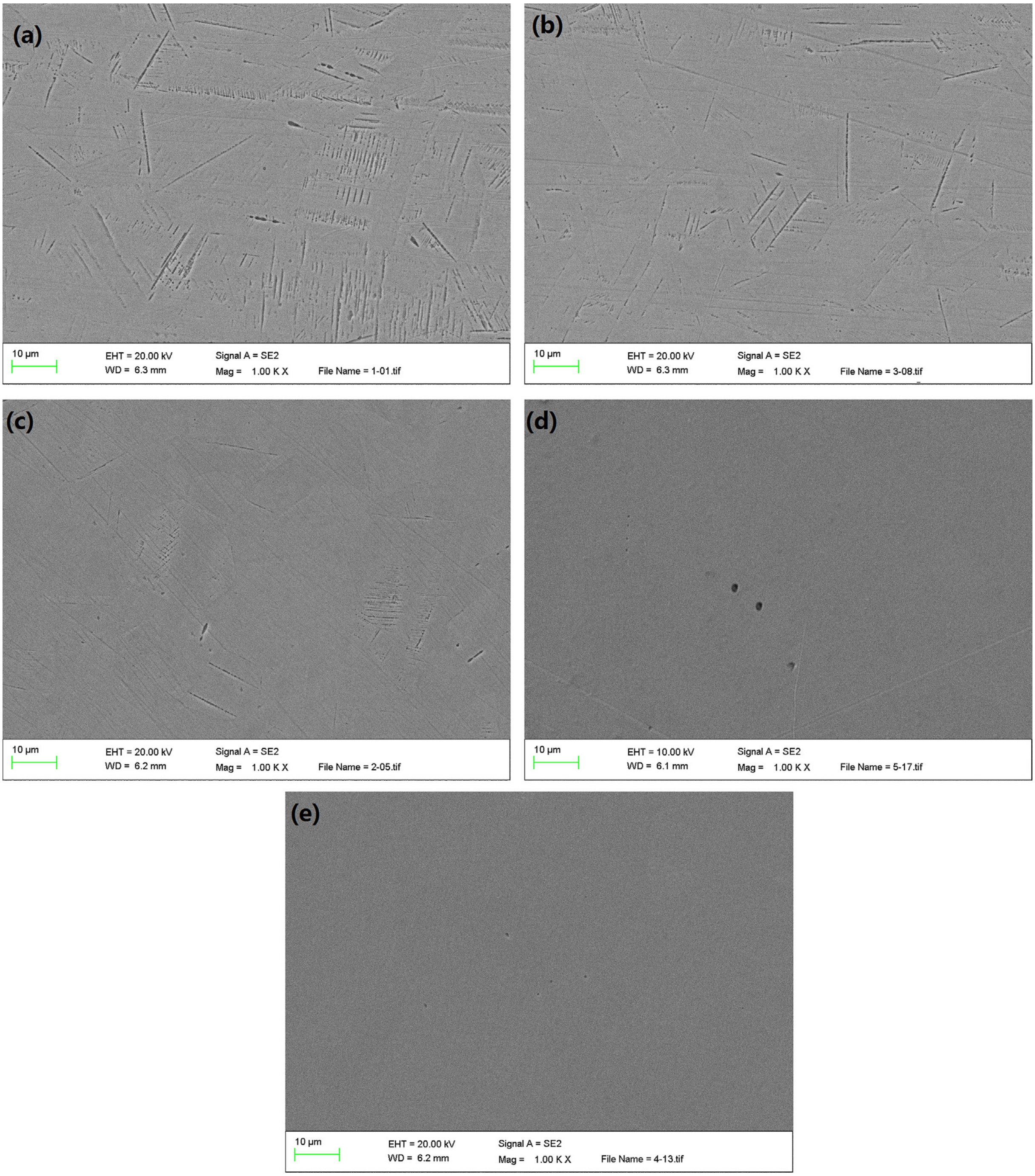

Fig. 3. SEM micrographs of the 304 SS polarised at −0.1 V for 10 h in 0.5 M H_2SO_4 + 2 ppm HF + x M CH_3OH (x = 0, 1, 5, 10 and 20) solutions at 50 °C: (a) without methanol; (b) 1 M methanol; (c) 5 M methanol; (d) 10 M methanol; (e) 20 M methanol.

region of log f vs log|Z| are less than −1, while the absolute value of the maximum phase angle is less than 90° due to the pseudocapacitive nature of the passive film [24]. In the low frequency range (below 1 Hz), a mass transfer process dominates the electrode impedance. From the above analyses and the SEM observations, an equivalent circuit, as illustrated in Fig. 5, is proposed to analyse the impedance spectra, where R_s represents the solution resistance between the electrolyte and working electrode; R_f and C_f represent the resistance and capacitance of the passive film layer [38,39], respectively; R_c and C_{dl} represent the charge transfer resistance and the double layer capacitance, respectively, and W represents the Warburg impedance. Due to the non-ideal capacitive response of the interface between the solution and sample, a constant phase element (CPE) is applied to replace both the C_f and C_{dl} for fitting the spectra. The impedance of the CPE can be denoted:

$$Z_{CPE} = Q(j\omega)^{-n} \tag{6}$$

where Q is the admittance magnitude of CPE, ω is the angular frequency, and n is the CPE power. The factor n is an adjustable parameter. When $n = 1$, Z_{CPE} equals the pure capacitance impedance. The pure resistor impedance is represented by $n = 0$.

Table 3
Metallic ions dissolved in the test solution containing different methanol concentrations after 10 h potentiostatic tests.

Methanol concentration	Dissolved ions concentration (ppm)			
	Fe	Cr	Ni	Total
0 M	7.3922	0.8653	0.6197	8.8772
1 M	7.0867	0.7685	0.6033	8.4585
5 M	6.0381	0.7257	0.5839	7.3477
10 M	5.1097	0.5128	0.4531	6.0756
20 M	5.0175	0.5101	0.4304	5.9580

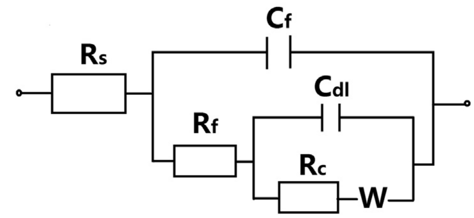

Fig. 5. Equivalent circuit for the corrosion system including the 304 SS/solution.

Practically, n lies between 0 and 1 [37,40]. Fig. 4 shows that the physical models are suitable to fit the experimental data very well, which would provide a reliable representation of the corrosion system. The fitted results are collected in Table 4. The solution resistances (R_s) increase with the methanol concentration, indicating a lower ionic conductivity in the solutions with higher methanol concentrations. R_f and Q_f decrease slightly and then tend to increase with the methanol concentration, most likely due to the change in the thickness and dielectric constant of the passive film formed on the 304 SS. The charge transfer resistance (R_c) represents the corrosion resistance of the materials; this value increases with the methanol concentration in the test solution. A higher R_c indicates a better corrosion resistance; the EIS results validate the results of the potentiodynamic and potentiostatic tests, showing that the methanol slows the corrosion rate of 304 SS under DMFC anodic operating conditions.

3.4. X-ray photoelectron spectroscopy

The passive film compositions of the 304 SS after 10 h potentiostatic tests in 0.5 M H_2SO_4 + 2 ppm HF + x M CH_3OH (x = 0, 1, 5, 10 and 20) solutions containing different methanol concentrations were identified by XPS. The depth profile results and Cr/Fe atomic ratios for the passive films are shown in Fig. 6(a)–(f). Based on the depth profiles and Cr/Fe atomic ratio, the Fe content is much lower in the passive film than that in the substrate due to its selective dissolution [36]. During the ICP–AES detections, the highest Fe ion concentration in the test solutions also reveals the selective

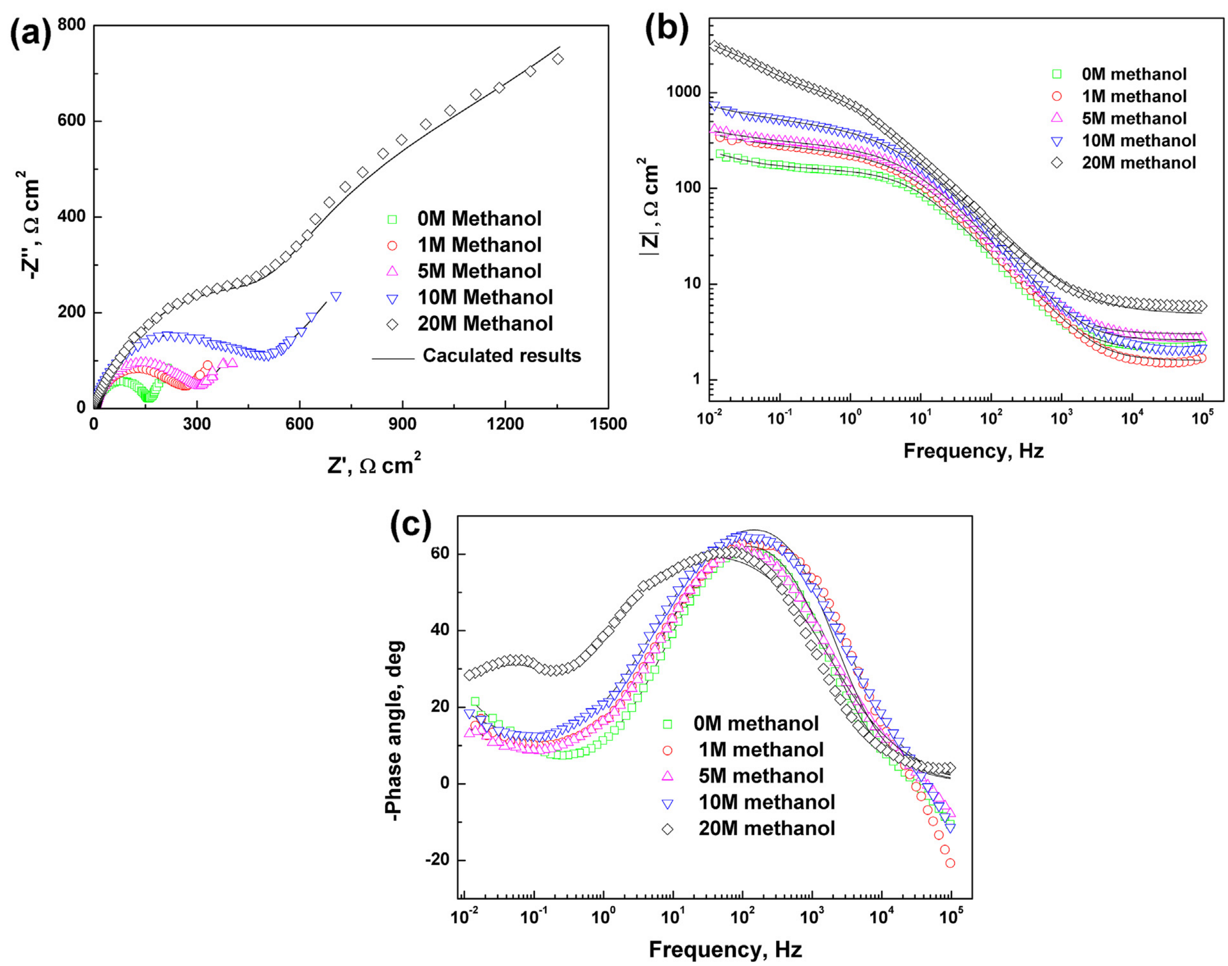

Fig. 4. Impedance plots for the 304 SS in 0.5 M H_2SO_4 + 2 ppm HF + x M CH_3OH (x = 0, 1, 5, 10 and 20) solutions at 50 °C: (a) Nyquist plots; (b) frequency–absolute plots; (c) frequency–angle plots. Symbols: experimental data; lines: fitted values.

Table 4
Fitted results for EIS spectra after 10 h potentiostatic tests in 0.5 M H_2SO_4 + 2 ppm HF + x M CH_3OH (x = 0, 1, 5, 10 and 20) solutions at 50 °C.

Methanol content	R_s (Ω cm^2)	Q_f (Ω^{-1} cm^{-2} s^{-n})	n_f	R_f (Ω cm^2)	Q_{dl} (Ω^{-1} cm^{-2} s^{-n})	n_{dl}	R_c (Ω cm^2)	W (Ω^{-1} s$^{-0.5}$ cm^{-2})
0 M	1.983	2.89×10^{-4}	0.7977	158.3	45.48×10^{-3}	0.7615	102.4	0.02745
1 M	1.589	8.639×10^{-5}	0.9016	6.221	3.371×10^{-4}	0.5843	252.3	0.02593
5 M	3.028	8.441×10^{-5}	0.897	1.442	2.918×10^{-4}	0.5465	296.3	0.02457
10 M	4.616	6.183×10^{-5}	0.9217	67.9	2.975×10^{-4}	0.5143	505.3	0.01224
20 M	4.858	2.364×10^{-4}	0.7232	1454	18.98×10^{-4}	0.8	1249	0.00231

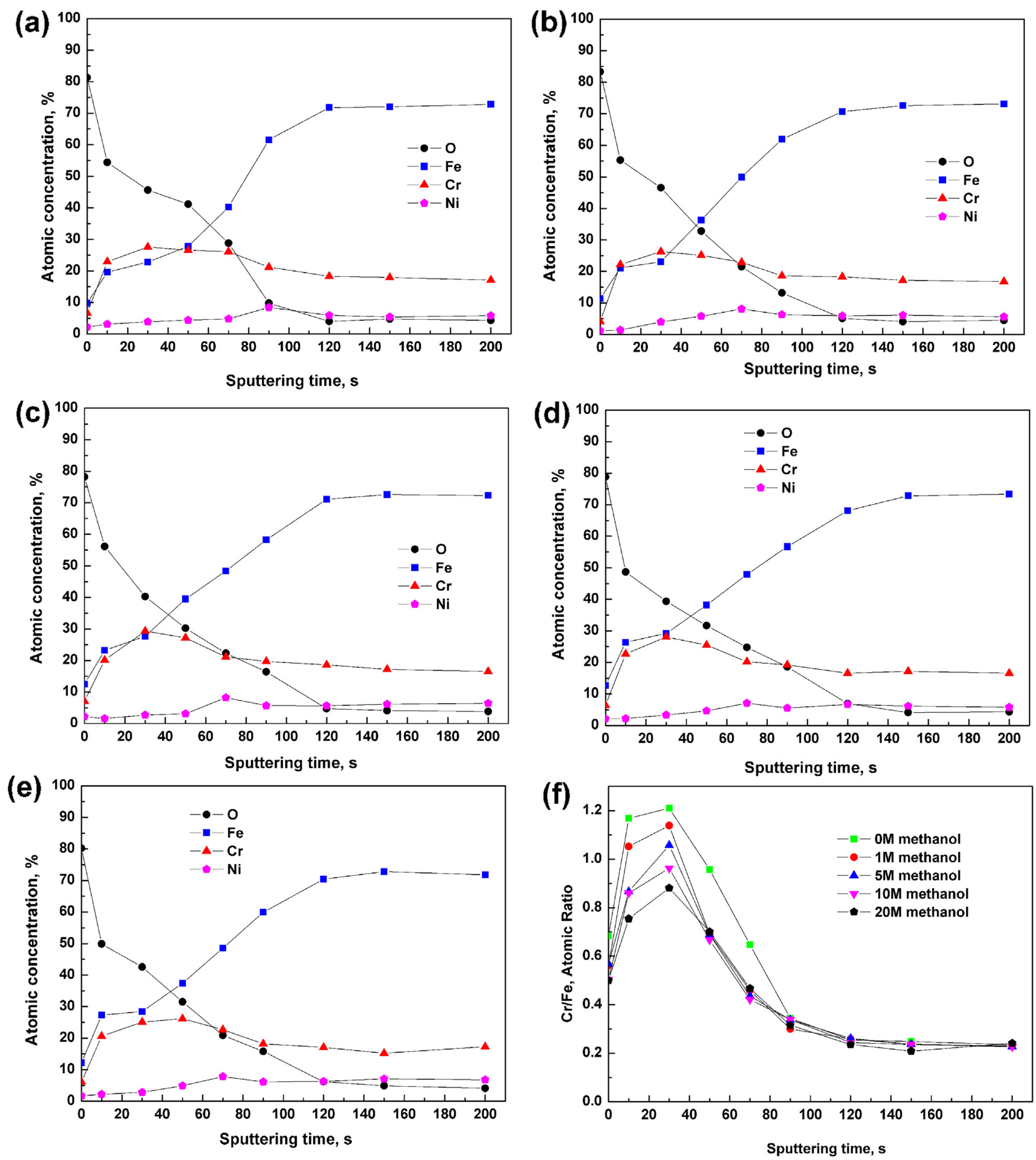

Fig. 6. XPS depth profiles of the passive film formed on the 304 SS polarised at −0.1 V for 10 h in 0.5 M H_2SO_4 + 2 ppm HF + x M CH_3OH (x = 0, 1, 5, 10 and 20) solutions at 50 °C: (a) 0 M methanol; (b) 1 M methanol; (c) 5 M methanol; (d) 10 M methanol; (e) 20 M methanol; (f) Cr/Fe atomic ratio.

dissolution behaviour of Fe in 304 SS. From the variation of Fe, Cr, and Ni compositions through the depth of the passive film, the passive film can be divided into two regions: in the external region of the passive film, the Fe content is higher than that of Cr due to the higher diffusion rate of Fe through the passive film [36]; a Cr-enriched layer is observed in the internal region of the passive film due to the selective dissolution and higher diffusion of Fe in the passive film. The Cr concentration reaches up to 26–30% in the passive film, exceeding that in stainless steel. Besides, it is noted, from the Cr to Fe ratios, that the Cr/Fe atomic ratio decreases as the methanol concentration increases in the test solutions at the same Ar ion sputtering time. Because the protic properties of the solutions (in addition to the dielectric constant and the dipole moment) decrease with increasing methanol concentrations, the iron ions are preferentially solvated by the available water molecules instead of by methanol, leading to the higher Fe content in the passive film formed in the test solutions with higher concentrations of methanol. A Ni-enriched layer is also found in the passive/metal interface region because the oxidation of Ni is more difficult than that of Fe and Cr in acid solutions [41]. Based on the XPS results, the passive film can be thought as being constitutive of two layers: an Fe dominant outer layer and a Cr-enriched inner layer, and the Fe content in the passive film is higher when the test solution contains a higher concentration of methanol. Moreover, the oxygen concentration decreases and subsequently stabilises as the sputtering time increases, indicating that the passive film is removed by the Ar ions and the substrate is sputtered. Considering the sputtering rate (approximately 0.06 nm s^{-1}), the oxide layer almost disappears after sputtering for approximately 80 s in the test solution without methanol, which suggests that the passive film thickness is approximately 4.8 nm. When increasing the methanol concentration in the test solution, more time is needed to remove the oxide layer. Therefore, it can be inferred that the thickness of the passive film would be slightly greater when the methanol content is higher, and the corresponding calculated thicknesses are approximately 4.8–5.4 nm, 5.4–6.0 nm, 6.0–6.6 nm and 6.6 nm when the test solution contains 1 M, 5 M, 10 M and 20 M methanol, respectively. The composition and thickness of the passive film dramatically affect the surface conductivity of the stainless steel, as will be discussed later.

3.5. Mott–Schottky analyses

The semi-conductive properties of the passive films formed on metals and alloys can be reflected by the capacitance curve as a function of the electrode potentials, which exhibits the charge distribution in the film [41]. In the present corrosion system, the measured capacitance is expected to be caused by the space charge capacitance (C), which depends on the applied electrode potential (E) via the Mott–Schottky equation [42]:

$$C^{-2} = \frac{2}{eN_d\varepsilon\varepsilon_0}\left(E - E_{fb} - \frac{kT}{e}\right) \quad (7)$$

for an n-type semiconductor and

$$C^{-2} = \frac{2}{-eN_a\varepsilon\varepsilon_0}\left(E - E_{fb} - \frac{kT}{e}\right) \quad (8)$$

for a p-type semiconductor, where e is the electron charge (1.602×10^{-19} C, $+e$ for holes and $-e$ for electrons); ε is the dielectric constant of the film (15.6 for a passive film formed on steel [43]); ε_0 is the vacuum permittivity (8.854×10^{-12} F m^{-1}); N_d and N_a are the donor and acceptor densities, respectively; E_{fb} is the flat band potential; k is the Boltzmann constant (1.38×10^{-23} J K^{-1}); and T is the absolute temperature. For an n-type semiconductor, the plot of C^{-2} vs E should be linear with a positive slope that is inversely proportional to the donor density. For a p-type semiconductor, the plot of C^{-2} vs E shows a negative slope that is inversely proportional to the acceptor density. The space charge capacitance (C) is calculated as $C = (-Z''2\pi f)^{-1}$, where f is the frequency and Z'' is the imaginary part of the impedance. Fig. 7 shows the Mott–Schottky plots for the passive films formed on the 304 SS after 10 h potentiostatic tests in 0.5 M H_2SO_4 + 2 ppm HF + x M CH_3OH (x = 0, 1, 5, 10 and 20) solutions with varied methanol concentrations. Duplex slopes of C^{-2} vs E curves can be observed in the Mott–Schottky plots. This phenomenon suggests that the passive films possess a duplex character with p- (negative slope) and n-type semiconductor behaviours (positive slope). However, the p-type semiconductor behaviour of the passive film formed on 304 SS in the acid solution containing 20 M methanol is not as pronounced as the p-type semiconductor behaviour observed for the other solutions due to the decreased dissolution of Fe, which behaves as an n-type semiconductor in its oxides [44], in the solution containing more methanol as indicated by the XPS data. The duplex property of the passive film with an n-type semiconductor outer layer and a p-type semiconductor inner layer has also been observed on stainless steel by other researchers using aqueous acid solutions [42–45]. The flat band potential (E_{fb}, the turning point of p-type to n-type semiconductor) and the carrier (donor and acceptor) density calculated from equations (7) and (8) for 304 SS in different solutions are presented in Table 5. When the applied potential (E) is higher than the E_{fb}, a depletion region would appear at the passive film–electrolyte interface, which would facilitate the outward migration of metal cations and the inward migration of anions and electrons at the passive film–electrolyte interface [30,45]. Table 5 shows that the E_{fb} of 304 SS increases with the methanol concentration, and the band bending decreases when the 304 SS samples are subjected to the same potential (−0.1 V). Thus, the 304 SS suffers less corrosion in the acid solution with higher methanol content, as indicated by the SEM observation. Moreover, a higher carrier (donor and acceptor) density means more defects, such as oxygen vacancies or cation vacancies, in the passive film [30], and less protection of the passive film. Table 5 shows that the carrier density decreases when the methanol concentration increases, suggesting that the methanol once again serves as the corrosion inhibitor for 304 SS in 0.5 M H_2SO_4 + 2 ppm HF solutions.

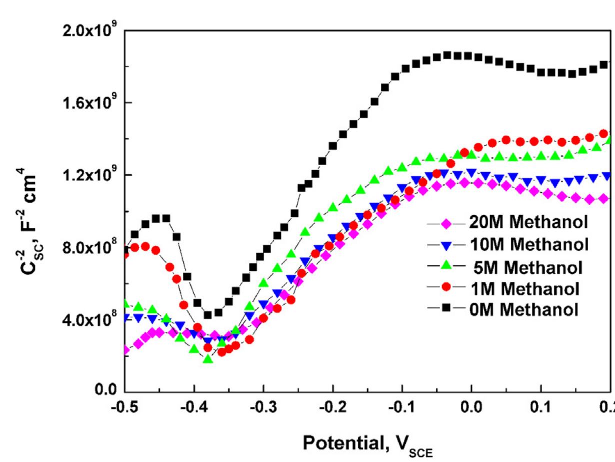

Fig. 7. Mott–Schottky plots for the passive films formed on 304 SS in 0.5 M H_2SO_4 + 2 ppm HF + x M CH_3OH (x = 0, 1, 5, 10 and 20) solutions at 50 °C.

Table 5
Flat band potential E_{fb} and carrier density for the semiconductor passive film formed on 304 SS after 10 h potentiostatic tests in 0.5 M H_2SO_4 + 2 ppm HF + x M CH_3OH (x = 0, 1, 5, 10 and 20) solutions at 50 °C.

Methanol content	Donor density (cm^{-3})	Acceptor density (cm^{-3})	E_{fb} (mV_{SCE})
0 M	1.259×10^{20}	6.121×10^{20}	−385
1 M	1.001×10^{20}	3.646×10^{20}	−380
5 M	0.759×10^{20}	0.883×10^{20}	−380
10 M	0.756×10^{20}	0.566×10^{20}	−375
20 M	0.592×10^{20}	0.284×10^{20}	−350

3.6. *Interfacial contact resistance*

The surface conductivity can be characterised by the ICR originating from contact between the bipolar plate and the gas diffusion layer, which has great effect on the performance of the DMFC stack. Fig. 8 presents the ICR of the 304 SS before and after the potentiostatic polarisation tests in the five different corrosion solutions. Clearly, the ICR after the potentiostatic tests are greater than the ICR before the tests. The XPS analyses suggest that the passive film formed on 304 SS is different from the iron oxides dominant air-formed oxide film. In addition, the conductivity of passive film decreases as the iron depleted in the passive film [3]. Therefore, the surface conductivity decreases when 304 SS is exposed to the DMFC anodic operating conditions. Furthermore, the 304 SS shows additional ICR increases in the solutions with higher methanol content due to the thicker passive film. At an applied compaction force of 140 N cm^{-2}, the ICRs of the 304 SS after the potentiostatic tests in 0.5 M H_2SO_4 + 2 ppm HF solutions containing 0 M, 1 M, 5 M, 10 M and 20 M methanol solutions are 180.3 mΩ cm^2, 186.2 mΩ cm^2, 200.8 mΩ cm^2, 212.6 mΩ cm^2 and 218.7 mΩ cm^2, respectively. Therefore, the methanol indirectly reduces the surface conductivity of 304 SS under DMFC anodic operating conditions.

4. Conclusions

The corrosion performance of the 304 SS under simulated DMFC anodic operating conditions (0.5 M H_2SO_4 + 2 ppm HF + x M CH_3OH (x = 0, 1, 5, 10 and 20) solutions at 50 °C) was systematically investigated. The results of potentiodynamic and potentiostatic polarisation as well as EIS show that the corrosion resistance of the 304 SS is better when the methanol content is higher. The corrosion current density, the critical current density and the passive current density decrease whereas the charge transfer resistance increases with the methanol concentration in the test solutions. After 10 h potentiostatic polarisation tests, 304 SS releases more metallic ions in the test solutions without methanol due to more severe inhomogeneous corrosion (intergranular corrosion, pitting and internal micro-stress corrosion). The XPS analyses reveal that the passive films formed on the 304 SS consist of an Fe-enriched outer layer and a Cr-enriched inner layer due to the selective dissolution and higher diffusion of Fe in the passive film. Moreover, the Fe content in the passive film increases as the methanol content increases because Fe ions are preferentially solvated by the available water molecules rather than methanol. The Mott–Schottky method not only confirms the duplex semiconductor behaviour of the passive film with an n-type semiconductor outer layer and a p-type semiconductor inner layer but also confirms that the corrosion resistance of 304 SS is enhanced with higher methanol contents by analysing the changes in the flat band potential (E_{fb}). Although the content of the more conductive iron oxide is increased in the passive film when the methanol concentration increases in the test solutions, the passive film thickness also increases, increasing the ICR.

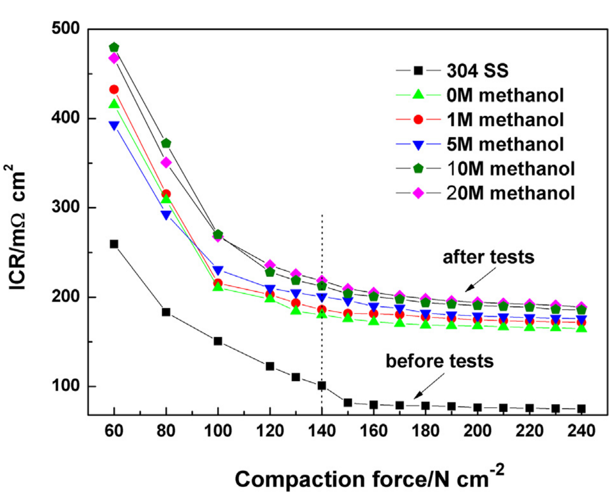

Fig. 8. ICR of 304 SS before and after the potentiostatic tests in 0.5 M H_2SO_4 + 2 ppm HF + x M CH_3OH (x = 0, 1, 5, 10 and 20) solutions at 50 °C.

Acknowledgements

This work is financially supported by The National Foundation of Natural Science of China (No. 21176034), Fundamental Research Funds for Team of Central Universities (No. 3132013314) and The Scientific Research Foundation for National Excellent Doctoral Dissertation Program (No. 2013YB02).

References

[1] C.E. Borroni-Bird, J. Power Sources 61 (1996) 33–48.
[2] M. Lefevre, E. Proietti, F. Jaouen, J.P. Dodelet, Science 324 (2009) 71–74.
[3] H. Wang, M.A. Sweikart, J.A. Turner, J. Power Sources 115 (2003) 243–251.
[4] L.X. Wang, J.C. Sun, P.B. Li, B. Jing, S. Li, Z.S. Wen, S.J. Ji, J. Power Sources 208 (2012) 397–403.
[5] M. Baldauf, W. Preidel, J. Power Sources 84 (1999) 161–166.
[6] S.V. Andrian, J. Meusinger, J. Power Sources 91 (2000) 193–201.
[7] Y. Liu, X. Xie, Y. Shang, R. Li, L. Qi, J. Guo, V.K. Mathur, J. Power Sources 164 (2007) 322–327.
[8] L. Sun, C. Liu, J. Liang, X. Zhu, T. Cui, J. Power Sources 196 (2011) 7533–7540.
[9] R.J. Tian, J.C. Sun, J. Power Sources 194 (2009) 981–984.
[10] R.J. Tian, J.C. Sun, L. Wang, J. Power Sources 163 (2007) 719–724.
[11] L.X. Wang, J.C. Sun, J. Sun, Y. Lv, S. Li, S.J. Ji, Z.S. Wen, J. Power Sources 199 (2012) 195–200.
[12] T.S. Zhao, R. Chen, W.W. Yang, C. Xu, J. Power Sources 191 (2009) 185–202.
[13] T. Bewer, T. Beckmann, H. Dohle, J. Mergel, D. Stolten, J. Power Sources 125 (2004) 1–9.
[14] C. Xie, J. Bostaph, J. Pavio, J. Power Sources 136 (2004) 55–65.
[15] Z. Yuan, Y. Zhang, J. Leng, Y. Gao, X. Liu, J. Power Sources 125 (2012) 134–142.
[16] J.H. Yoo, H.G. Choi, J.E. Nam, Y. Lee, C.H. Chung, E.S. Lee, J.K. Lee, S.M. Cho, J. Power Sources 158 (2006) 13–17.
[17] Z. Guo, A. Faghri, J. Power Sources 160 (2006) 1183–1194.
[18] M.A. Abdelkareem, N. Nakagawa, J. Power Sources 162 (2006) 114–123.
[19] X. Li, A. Faghri, C. Xu, Int. J. Hydrogen Energy 35 (2010) 8690–8698.
[20] N. Nakagawa, T. Tsujiguchi, S. Sakurai, R. Aoki, J. Power Sources 219 (2012) 325–332.
[21] M. Kumagai, S.T. Myung, S. Kuwata, R. Asaishi, H. Yashiro, Electrochim. Acta 53 (2008) 4205–4212.
[22] A. Pozio, R.F. Silva, M.D. Francesco, L. Giorgi, Electrochim. Acta 48 (2003) 1543–1549.
[23] P.L. Anna, Corros. Sci. 25 (1985) 43–53.
[24] M. Ray, V.B. Singh, J. Electrochem. Soc. 158 (11) (2011) C359–C368.
[25] F. Mansfeld, J. Electrochem. Soc. 120 (1973) 188–192.
[26] J. Banns, Corros. Sci. 22 (1982) 1005–1013.
[27] V.K. Singh, V.B. Singh, Corros. Sci. 28 (1988) 385–395.
[28] D. Shintani, T. Ishida, H. Izumi, T. Fukutsuka, Y. Mastsuo, Y. Sugie, Corros. Sci. 50 (2008) 2840–2845.
[29] E. Heitz, M. Fontana, R. Staehle (Eds.), Advances in Corrosion Science and Technology, Plenum Press, New York, 1974, pp. 149–243.
[30] Y. Yang, L. Guo, H. Liu, J. Power Sources 195 (2010) 5651–5659.
[31] T. Kavai, H. Nishihara, K. Aramaki, Corros. Sci. 37 (1995) 823–831.
[32] Z. Stein, E. Gileadi, J. Electrochem. Soc. 132 (1985) 2166–2171.
[33] C.S. Brossia, E. Gileadi, R.G. Kelly, Corros. Sci. 37 (1995) 1455–1471.

[34] M. Sakakibara, N. Saito, H. Nishihara, K. Aramaki, Corros. Sci. 34 (1993) 391–402.
[35] G.O. Mepsed, J.M. Moore, Handbook of Fuel Cell: Fundamentals, Technology, and Applications, John Wiley and Sons, Ltd., New York, 2003, pp. 286–293.
[36] C.O.A. Olsson, D. Landolt, Electrochim. Acta 48 (9) (2003) 1093–1104.
[37] X. Wu, H. Ma, S. Chen, Z. Xu, A. Sui, J. Electrochem. Soc. 146 (5) (1999) 1847–1853.
[38] I. Frateur, C. Deslouis, M.E. Orazem, B. Tribollet, Electrochim. Acta 44 (1999) 4345–4356.
[39] K. Juttner, W.J. Loronz, J. Electrochem. Soc. 135 (1988) 332–339.
[40] C.H. Hsu, F. Mansfeld, Corrosion 57 (2001) 747–748.
[41] L. Liu, Y. Li, F. Wang, Electrochim. Acta 52 (2007) 2392–2400.
[42] N.E. Hakiki, M.F. Montemor, M.G.S. Ferreira, M.C. Belo, Corros. Sci. 42 (2000) 687–702.
[43] D.D. Macdonald, J. Electrochem. Soc. 153 (2006) B213–B224.
[44] H. Tsuchiya, S. Fujimoto, O. Chihara, T. Shibata, Electrochim. Acta 47 (2002) 4357–4366.
[45] R. Jiang, C. Chen, S. Zheng, Electrochim. Acta 55 (2010) 2498–2504.